

Are your MRI contrast agents cost-effective?

Learn more about generic Gadolinium-Based Contrast Agents.



FRESENIUS  
KABI

caring for life

# AJNR

## **Radiomics-Based Machine Learning for Outcome Prediction in a Multicenter Phase II Study of Programmed Death-Ligand 1 Inhibition Immunotherapy for Glioblastoma**

E. George, E. Flagg, K. Chang, H.X. Bai, H.J. Aerts, M. Vallières, D.A. Reardon and R.Y. Huang









This information is current as of April 23, 2024.

*AJNR Am J Neuroradiol* 2022, 43 (5) 675-681

doi: <https://doi.org/10.3174/ajnr.A7488>

<http://www.ajnr.org/content/43/5/675>

# Radiomics-Based Machine Learning for Outcome Prediction in a Multicenter Phase II Study of Programmed Death-Ligand 1 Inhibition Immunotherapy for Glioblastoma

 E. George,  E. Flagg,  K. Chang,  H.X. Bai,  H.J. Aerts,  M. Vallières,  D.A. Reardon, and  R.Y. Huang



## ABSTRACT

**BACKGROUND AND PURPOSE:** Imaging assessment of an immunotherapy response in glioblastoma is challenging due to overlap in the appearance of treatment-related changes with tumor progression. Our purpose was to determine whether MR imaging radiomics-based machine learning can predict progression-free survival and overall survival in patients with glioblastoma on programmed death-ligand 1 inhibition immunotherapy.

**MATERIALS AND METHODS:** Post hoc analysis was performed of a multicenter trial on the efficacy of durvalumab in glioblastoma ( $n=113$ ). Radiomics tumor features on pretreatment and first on-treatment time point MR imaging were extracted. The random survival forest algorithm was applied to clinical and radiomics features from pretreatment and first on-treatment MR imaging from a subset of trial sites ( $n=60-74$ ) to train a model to predict long overall survival and progression-free survival and was tested externally on data from the remaining sites ( $n=29-43$ ). Model performance was assessed using the concordance index and dynamic area under the curve from different time points.

**RESULTS:** The mean age was 55.2 (SD, 11.5) years, and 69% of patients were male. Pretreatment MR imaging features had a poor predictive value for overall survival and progression-free survival (concordance index = 0.472–0.524). First on-treatment MR imaging features had high predictive value for overall survival (concordance index = 0.692–0.750) and progression-free survival (concordance index = 0.680–0.715).

**CONCLUSIONS:** A radiomics-based machine learning model from first on-treatment MR imaging predicts survival in patients with glioblastoma on programmed death-ligand 1 inhibition immunotherapy.

**ABBREVIATIONS:** AUC = area under the curve; C-index = concordance index; ET = enhancing tumor; IQR = interquartile range; OS = overall survival; PFS = progression-free survival; PD-1 = programmed cell death protein 1; PD-L1 = programmed death-ligand 1; WT = whole tumor


Glioblastoma is the most common primary malignant brain tumor among adults.<sup>1</sup> The current standard of care is maximal surgical resection followed by radiation and temozolomide chemotherapy. However, eventual progression of the tumor is typical with limited further treatment options and a dismal median overall survival (OS) of 15 months and 5-year survival of

<10%.<sup>2</sup> Despite advances in the understanding of molecular changes in glioblastoma, effective targeted therapies are lacking, and bevacizumab, a monoclonal antibody against the vascular

The clinical study was funded by Medimmune, the Cancer Research Institute, and the Ludwig Institute for Cancer Research. Dr Huang received support from the American Roentgen Ray Society/American Society of Neuroradiology Scholar grant. Dr George received support from the American Society of Neuroradiology Scholar Award. Dr Bai received support from the Radiological Society of North America Scholar grant. Research reported in this publication was supported by a training grant from the National Institute of Biomedical Imaging and Bioengineering of the National Institutes of Health under award No. 5T32EB1680 and by the National Cancer Institute of the National Institutes of Health under award No. F30CA239407 to Dr Chang and by the National Cancer Institute of the National Institutes of Health under Award No. R03CA249554 to Dr Bai. Dr Vallières acknowledges funding from the Canada CIFAR AI Chairs Program.

Please address correspondence to Raymond Y. Huang, MD, PhD, Department of Radiology, Brigham and Women's Hospital, 75 Francis St, Boston, MA 02115; e-mail: ryhuang@bwh.harvard.edu; @LizzRad

 Indicates open access to non-subscribers at [www.ajnr.org](http://www.ajnr.org)

 Indicates article with online supplemental data.

<http://dx.doi.org/10.3174/ajnr.A7488>

Received October 20, 2021; accepted after revision February 17, 2022.

From the Department of Radiology and Biomedical Imaging (E.G.), University of California San Francisco, San Francisco, California; Department of Radiology (E.F., R.Y.H.), Brigham and Women's Hospital, Boston, Massachusetts; Massachusetts Institute of Technology (K.C.), Cambridge, Massachusetts; Department of Diagnostic Imaging (H.X.B.), Rhode Island Hospital and Warren Alpert Medical School of Brown University, Providence, Rhode Island; Artificial Intelligence in Medicine Program (H.J.A.), Brigham and Women's Hospital, Harvard Medical School, Boston, Massachusetts; Departments of Radiation Oncology and Radiology (H.J.A.), Brigham and Women's Hospital, Dana-Farber Cancer Institute, Harvard Medical School, Boston, Massachusetts; Department of Computer Science (M.V.), Université de Sherbrooke, Sherbrooke, Quebec, Canada; and Center for Neuro Oncology (D.A.R.), Dana-Farber Cancer Institute, Boston, Massachusetts.

E. George and E. Flagg contributed equally to the study.

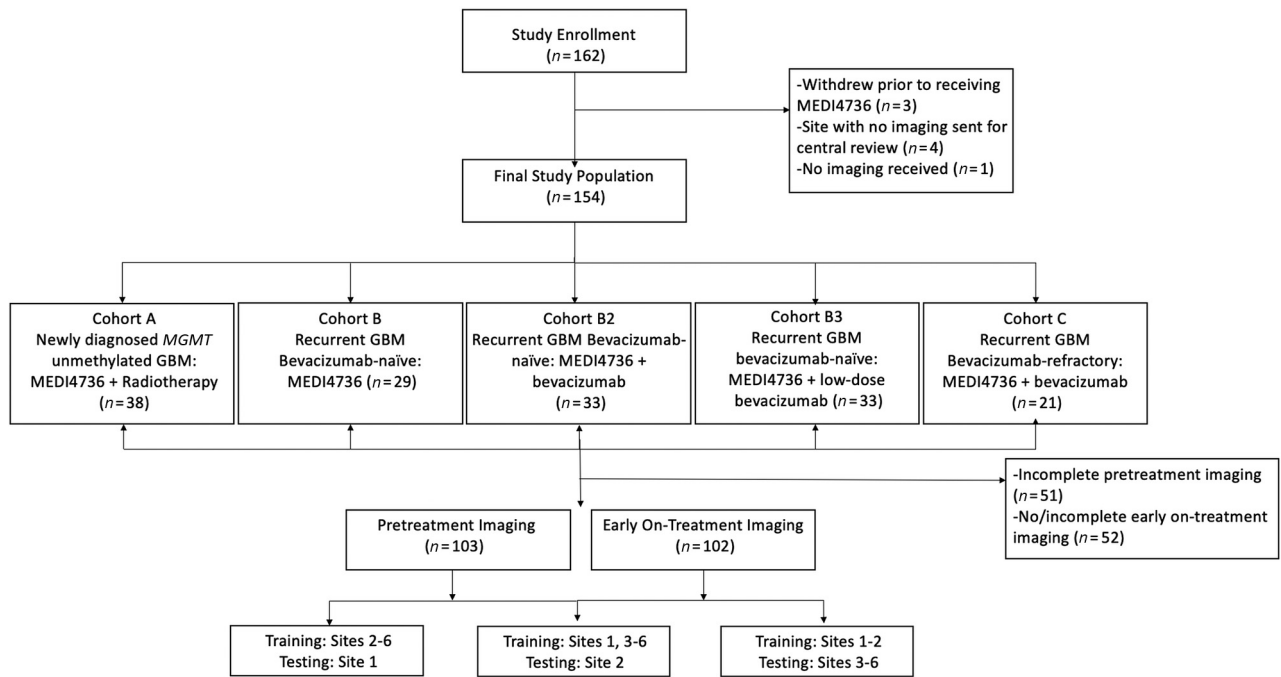


**FIG 1.** Flow chart of the study population.

endothelial growth factor, is the only approved addition to recurrent glioblastoma management.<sup>3</sup>

Preclinical studies of programmed cell death protein 1 (PD-1) pathway inhibition showed promising results in glioma.<sup>4,5</sup> However, in clinical trials, PD-1 inhibition via nivolumab concurrently with chemoradiotherapy or radiation therapy did not improve progression-free survival (PFS) or OS in newly diagnosed glioblastoma<sup>6,7</sup> or improve OS compared with bevacizumab in recurrent glioblastoma.<sup>8</sup> Although the overall response rate to nivolumab was low (8%) in patients with recurrent glioblastoma, the response was more durable relative to bevacizumab.<sup>8</sup> Durvalumab (MEDI4736) is a monoclonal antibody against human programmed death-ligand 1 (PD-L1) that has shown clinical efficacy with an acceptable safety profile<sup>9</sup> and is being studied in multiple cancer subtypes, including glioblastoma.

Imaging assessments in glioma are challenging due to the overlap in the appearance of treatment-related changes with tumor progression, particularly in the setting of multimodality treatment.<sup>10,11</sup> Considering the possible low response rate to immunotherapy<sup>12</sup> and the poor median OS in glioblastoma, imaging-based metrics to predict response and improved survival early are desirable to make appropriate treatment decisions. Radiomics methods enable quantification of multisequence imaging data from spatially heterogeneous tissues, and machine learning techniques allow integration of these multiple quantitative metrics.

Here, we performed a post hoc analysis of a multicenter Phase II study (NCT02336165) of patients with glioblastoma undergoing durvalumab therapy with MR imaging radiomics and machine learning techniques. The aim of this study was to determine whether MR imaging radiomics-based machine learning can predict PFS and OS in patients with glioblastoma on PD-L1 inhibition immunotherapy.

## MATERIALS AND METHODS

This was a post hoc analysis of data from a Phase II clinical trial to evaluate the clinical efficacy and safety of durvalumab (MEDI4736) in glioblastoma (NCT02336165) conducted at 8 sites (7 in the United States, 1 in Australia) and enrolling 162 patients between March 2015 and January 2017 into 5 noncomparative patient cohorts (Fig 1 and Online Supplemental Data). The Online Supplemental Data summarize the trial inclusion/exclusion criteria. The institutional review board (Dana-Farber Cancer Institute) approved this trial, and all patients provided written informed consent. Of the 162 patients enrolled, 3 did not receive MEDI4736 due to clinical decline ( $n=1$ ), seizure ( $n=1$ ), or withdrawal of consent ( $n=1$ ) before drug administration (Fig 1).

### Imaging

MR imaging was performed approximately every 2 months during treatment, once during on-study follow-up, and at least every 6 months during poststudy follow-up. Brain MR imaging was performed on 1.5T or 3T scanners before and after the administration of gadolinium-based contrast media. Brain MR imaging protocol included sagittal and/or axial T1-weighted images, axial T2, axial T2-FLAIR, postcontrast axial or coronal fast spin-echo or 3D T1-weighted gradient-echo images, and susceptibility weighted imaging (Online Supplemental Data).

Imaging data were not available for central review for the Australian site ( $n=4$ ) and for 1 US patient ( $n=1$ ); hence, these were excluded. For this study, imaging performed pretreatment and at the first on-treatment time point was analyzed. First on-treatment MR imaging refers to the first MR imaging obtained after starting treatment and was performed approximately 8 weeks after initiation of treatment. Only patients with complete T1 pre-contrast, T2, T2-FLAIR, and T1 postcontrast imaging were included in the study for each time point (Fig 1).

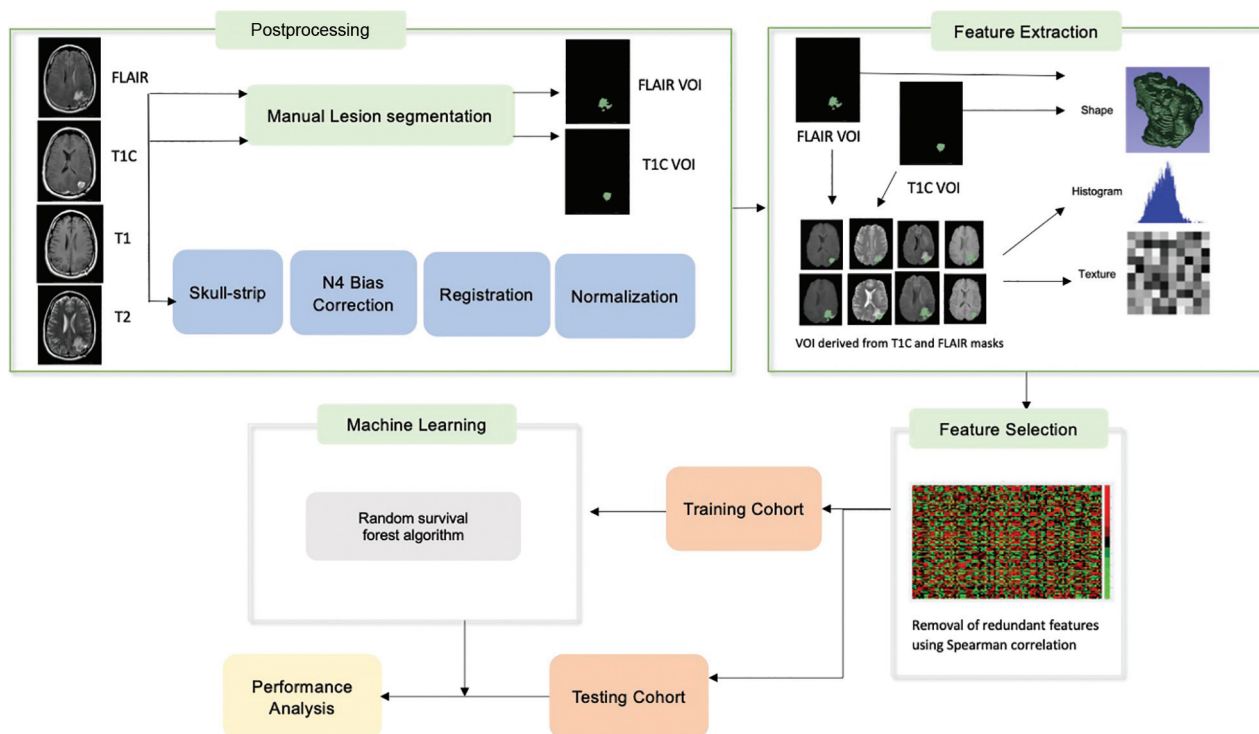


**FIG 2.** Radiomics and machine learning workflow. TIC indicates T1 post contrast imaging.

Progression was defined on the basis of the modified Response Assessment in Neuro-Oncology criteria<sup>13,14</sup> if the patient met any one of the following criteria:

1. A 25% increase in the sum of the products of perpendicular diameters of enhancing lesions (over best response or baseline if no decrease) on stable or increasing doses of corticosteroids
2. Any new lesion
3. Clear clinical deterioration not attributable to other causes apart from the tumor
4. Failure to return for evaluation due to death or deteriorating condition.

Patients with suspected progression were permitted to continue therapy at least until confirmation of progression on follow-up imaging in 8 weeks.

### Image Postprocessing

Image postprocessing methods are reported per the Image Biomarker Standardization Initiative guidelines (Online Supplemental Data).<sup>15</sup> The T2-FLAIR images were used to segment the whole tumor (WT) VOI, which includes enhancing tumor, infiltrating tumor, and vasogenic edema while postcontrast T1 images were used to determine the enhancing tumor (ET) VOI on the pretreatment and first on-treatment time point MR imaging. For segmentation, we used a semiautomated level tracing tool on 3D Slicer, Version 4.4 (<http://www.slicer.org>). All included imaging sequences (T2, T2-FLAIR, T1, T1 postcontrast) were skull-stripped,<sup>16</sup> and image intensities were corrected for low-frequency intensity nonuniformity via N4 bias field correction. Image intensities were then normalized using the median

and interquartile range (IQR) of image intensities<sup>17</sup> of the normal brain VOI (defined as the region outside the WT VOI, Fig 2) using Matlab (R2015a; MathWorks). All imaging sequences were resampled to 1 mm and spatially registered to the T1 postcontrast images using rigid followed by affine transformation with the Matlab Imaging Processing Toolbox.

### Radiomics Feature Extraction and Feature Selection

The radiomics feature extraction was performed using Matlab and included features from the open-source radiomics package by Vallières et al<sup>18,19</sup> (Online Supplemental Data). In this package, 3 feature categories were included to characterize the tumor shape (10 features), intensity histogram (18 features each for 4 sequences [T1, T2, T2-FLAIR, T1 postcontrast]), and texture (40 features each for the aforementioned 4 sequences).<sup>18,20</sup> A total of 242 features were included for each VOI (WT and ET) for a total of 484 imaging features for each time point in addition to 5 clinical features of age, race, sex, study site, and treatment regimen. The treatment regimen was included as a feature to account for the heterogeneity in population (newly diagnosed versus recurrent glioblastoma and durvalumab monotherapy versus combination therapy).

Feature selection was performed using feature variability and redundancy. Feature variability, a measure of stability, was assessed as the percentage difference between the feature value before and after shifting the tumor VOI 3 voxels in all directions. The variability for each feature was obtained for each case and then averaged over all cases to obtain the average feature variability for each feature. Features with a variability of >150% were removed. Next, redundant features, defined as features with a

Spearman correlation of  $>0.8$ ,  $P < .05$  with another feature, were removed.

### Radiomics Model Training

The random survival forest algorithm<sup>21</sup> was applied using the scikit-survival 0.17.1 Python module.<sup>22</sup> Censored survival data (see Statistical Analysis section) including event (death or progression) and time to event were input into the algorithm along with the selected feature set. Tuning of hyperparameters was performed using a grid search, and the optimized parameters are included in the Online Supplemental Data.

### Radiomics Model Performance

To assess the generalizability of radiomics models across multiple centers, we designed 3 separate experiments using data from different sites for model training and model testing, while keeping the ratio of the number of patients in training and testing groups to about 2–3:1 (Fig 1 and Online Supplemental Data). After each model was trained using the “training” group, the model performance was evaluated in an intentionally withheld external “testing” group.

1. Training with sites 2–6 ( $n = 70$ – $72$ ) and testing with site 1 ( $n = 31$ – $32$ )
2. Training with sites 1 and 3–6 ( $n = 73$ – $74$ ) and testing with site 2 ( $n = 29$ )
3. Training with sites 1 and 2 ( $n = 60$ – $61$ ) and testing with sites 3–6 ( $n = 41$ – $43$ ).

These experiments were conducted separately for pretreatment and first on-treatment MR imaging–derived features (combined with clinical variables, Online Supplemental Data). Model performance was assessed using both the concordance index (C-index) and dynamic area under the curve (AUC) for different time points.<sup>23</sup>

### Top-Performing Features

For each experiment, the top 20 features were reported along with their corresponding weights in the trained model (Online Supplemental Data). The top features were calculated using “out of bag” samples, which are sets of outcomes in the training set that are randomly excluded from model training. This step avoids overlap with the training data when analyzing the strength of a given feature.

### Statistical Analysis

Overall survival was defined as the time from therapy initiation to death, and progression-free survival was defined as the time from therapy initiation to progression of disease. If the patient was alive at the last follow-up, the OS was censored at the time of last clinical follow-up; in patients with stable or improved disease at last follow-up, PFS was censored at the last imaging follow-up. These results are based on the data lock date of November 20, 2019, for OS and September 6, 2019, for PFS. The accuracy of the model was assessed using the C-index and dynamic AUC for different time points. Statistical analyses used Python, Version 3.7.6.

**Table 1: Patient characteristics**

| Characteristics         | <i>n</i> = 113      |
|-------------------------|---------------------|
| Age (mean) (yr)         | 55.2 (SD, 11.5)     |
| Male (No.) (%)          | 78 (69%)            |
| Race                    |                     |
| White                   | 99 (87.6%)          |
| African American        | 1 (0.9%)            |
| Asian                   | 1 (0.9%)            |
| Other                   | 3 (2.7%)            |
| Unknown                 | 9 (8.0%)            |
| Treatment regimen       |                     |
| Cohort A                | 30 (26.5%)          |
| Cohort B                | 26 (23.0%)          |
| Cohort B2               | 23 (20.4%)          |
| Cohort B3               | 19 (16.8%)          |
| Cohort C                | 15 (13.3%)          |
| Median PFS (IQR) (days) | 106 (56–150.5)      |
| Median OS (IQR) (days)  | 207.5 (150.5–393.5) |

## RESULTS

### Patient Characteristics

A total of 113 patients with complete imaging of the 154 enrolled in this trial were included in this analysis, including 103 patients who had complete pretreatment imaging and 102 who had complete first on-treatment imaging (Fig 1). The demographics and treatment regimen of the included patients are presented in Table 1. Of the 113 patients included in the study, 103 had progression (median PFS = 106 days; IQR = 56–150.5 days) and the remaining 10 were censored at the last imaging follow-up available. Ninety of the 113 patients died during follow-up (median OS = 207.5 days; IQR = 150.5–393.5 days), and the remaining 23 were censored at the last clinical follow-up.

The median time from pretreatment imaging to the start of treatment was 7 days (IQR = 6–14 days) and from the start of treatment to first on-treatment imaging was 55.5 days (IQR = 54–56 days).

### Radiomics Model Performance

After we removed high-variability features and redundant features from the original 489 features, the pretreatment models each included 162–267 features and the first on-treatment models included 168–200 features. The radiomics models trained using pretreatment imaging features showed poor performance in predicting OS and PFS (C-index = 0.472–0.521 for OS and C-index = 0.472–0.524 for PFS in the testing cohort). Conversely, the radiomics models trained using first on-treatment imaging features showed a high C-index for the prediction of OS in the out of bag training cohort (C-index = 0.690–0.721) and testing cohort (C-index = 0.692–0.750, Table 2). Dynamic AUC plots for the first on-treatment models predicting OS (Online Supplemental Data) showed a peak AUC between 300 and 600 days postenrollment.

The first on-treatment imaging features–based radiomics model also showed a high C-index for the prediction of PFS in the out of bag training (C-index = 0.641–0.660) cohort and in the testing cohort (C-index = 0.680–0.715, Table 2). Dynamic AUC plots for the first on-treatment models predicting PFS showed variable AUC peak times, ranging from approximately 125 to 400 days.



**Table 2: Radiomics model performance for prediction of OS and PFS**

| Outcome/ MR Imaging Time Point | Training Site      | Testing Site         | OOB Training, Mean C-Index (95% CI) | Testing AUC, Mean C-Index (95% CI) |                     |
|--------------------------------|--------------------|----------------------|-------------------------------------|------------------------------------|---------------------|
| OS                             | Pretreatment       | Sites 2–6 (n = 72)   | Site 1 (n = 31)                     | 0.471 (0.467–0.474)                | 0.521 (0.515–0.527) |
|                                |                    | Site 1, 3–6 (n = 74) | Site 2 (n = 29)                     | 0.523 (0.517–0.530)                | 0.472 (0.468–0.476) |
|                                |                    | Site 1–2 (n = 60)    | Site 3–6 (n = 43)                   | 0.529 (0.526–0.532)                | 0.485 (0.483–0.488) |
|                                | First on-treatment | Sites 2–6 (n = 70)   | Site 1 (n = 32)                     | 0.690 (0.688–0.692)                | 0.750 (0.747–0.753) |
|                                |                    | Site 1, 3–6 (n = 73) | Site 2 (n = 29)                     | 0.710 (0.708–0.713)                | 0.748 (0.744–0.752) |
|                                |                    | Site 1–2 (n = 61)    | Site 3–6 (n = 41)                   | 0.721 (0.719–0.723)                | 0.692 (0.691–0.694) |
| PFS                            | Pretreatment       | Sites 2–6 (n = 72)   | Site 1 (n = 31)                     | 0.469 (0.467–0.472)                | 0.524 (0.518–0.530) |
|                                |                    | Site 1, 3–6 (n = 74) | Site 2 (n = 29)                     | 0.521 (0.515–0.526)                | 0.472 (0.469–0.476) |
|                                |                    | Site 1–2 (n = 60)    | Site 3–6 (n = 43)                   | 0.528 (0.524–0.531)                | 0.486 (0.484–0.488) |
|                                | First on-treatment | Sites 2–6 (n = 70)   | Site 1 (n = 32)                     | 0.660 (0.658–0.663)                | 0.691 (0.688–0.693) |
|                                |                    | Site 1, 3–6 (n = 73) | Site 2 (n = 29)                     | 0.641 (0.640–0.643)                | 0.715 (0.712–0.717) |
|                                |                    | Site 1–2 (n = 61)    | Site 3–6 (n = 41)                   | 0.648 (0.645–0.650)                | 0.680 (0.677–0.683) |

**Note:**—OOB indicate out of bag.

### Top-Performing Features

Because the models trained using first on-treatment MR imaging features had the best performance, they were used for determination of top-performing features. In each experiment with first on-treatment MR imaging features, the 20 top-performing features were predominantly texture features with a few shape features included (Online Supplemental Data). The treatment regimen was feature 12 of 20 in one of the models (Online Supplemental Data), but it was not a top-performing feature in any of the other first on-treatment models. Demographics and study site were not included in the top features for any of the first on-treatment models.

### DISCUSSION

There is a need for identification of specific imaging features for response assessment and reliable imaging-based prognostic markers in glioblastoma. Our multicenter study demonstrates that a radiomics model combining first on-treatment MR imaging features and clinical variables can accurately predict OS and PFS on durvalumab PD-L1 inhibition immunotherapy. The results were consistent across treatment sites with heterogeneous imaging protocols as confirmed by site-specific analysis with independent testing.

An increasing number of clinical trials are evaluating immunotherapy approaches for malignant glioma, but there are limited data assessing machine learning-based or other quantitative methods for imaging-based prognosis in patients with gliomas on immunotherapy. Radiomics prediction of survival on PD-L1 inhibition immunotherapy has previously been studied in other malignancies, including bladder cancer<sup>24</sup> and non-small-cell lung cancer.<sup>25</sup> In glioma, previous work has used radiomics features and machine learning to predict PD-L1 expression and subsequently found that the predicted high PD-L1 subgroup correlated with better prognosis.<sup>26</sup> There is also an extensive body of literature that has assessed the role of machine learning in various other aspects of glioma imaging,<sup>27</sup> including determination of glioma grade,<sup>28</sup> genomic status,<sup>29</sup> segmentation,<sup>30</sup> and prediction of survival.<sup>31</sup> Radiomics-based supervised machine learning algorithms have shown that shape and texture features extracted from

conventional and advanced MR images can predict survival in gliomas of varying grades.<sup>32,33</sup> In recurrent glioblastoma treated with bevacizumab, pretreatment texture and volumetric features were predictive of progression and survival.<sup>34,35</sup> However, in recurrent high-grade gliomas treated with bevacizumab and radiation, posttherapy scan texture features were predictive of overall survival.<sup>36</sup> Despite the differences in study populations, these models are similar to our results in which 75%–85% of top-performing first on-treatment features were texture features (Online Supplemental Data). A combination of deep and supervised learning using clinical features, tumor location, size, and features extracted from postcontrast T1 images, fMRI, and DTI have also been successful in predicting survival accurately in newly diagnosed glioblastoma.<sup>37</sup>

Our study identified texture features from all conventional imaging sequences for both enhancing and WT volume contributory to predicting survival from first on-treatment MR imaging. Our goal using first on-treatment MR imaging was to assess immunotherapy-related imaging changes as opposed to progression-related changes because progression timelines and types vary across the dataset. The predictive value of first on-treatment imaging features may reflect biologic differences in responders versus nonresponders to immunotherapy, including molecular alterations and changes in immune expression and infiltration.<sup>38</sup> The heterogeneity of the study population and integration of varied imaging protocols are strengths of the study. Similar out-of-bag and testing C-index values in each of the site-specific first-on-treatment analyses demonstrate that the first on-treatment imaging feature-based prediction model is generalizable (Table 2).

Although overall survival in the durvalumab study was low, with a median survival of 208 days, 20% of the study population was alive at the time of last follow-up. The response rate to immunotherapy in solid and hematologic malignancies is also reported to be 20%–30%.<sup>39</sup> Although the efficacy of checkpoint inhibitors in glioblastoma is unclear, preliminary results suggest a durable response in a small subset of patients.<sup>40</sup> Early imaging-based biomarkers that predict response to immunotherapy<sup>41</sup> can inform clinical decision-making.

Our study has several limitations. The relatively small sample size is a limitation, and the results need verification in larger

prospective trials and assessment for generalizability to other immune checkpoint inhibitors. The sample size also did not allow us to analyze advanced MR imaging variables such as DWI/ADC or perfusion and various molecular alterations or study the radiomics features in individual treatment regimens or progression patterns separately. Instead, the treatment regimen was included as a variable in the random forest survival analysis, where it was among the top-performing features in only one of the first on-treatment models. In a larger checkpoint inhibitor trial, we hope to conduct similar experiments to further investigate the impact of treatment variation on model performance, expand on this work to train models based on distinct progression mechanisms, and validate results across other checkpoint inhibitors. Last, while the variation in image-acquisition parameters in this study supports the potential generalizability of the model, it also limits the reproducibility of the imaging dataset used for model training.

## CONCLUSIONS

We created and validated a robust machine learning model for prediction of OS and PFS in patients with glioblastoma on PD-L1 inhibition immunotherapy using first on-treatment MR imaging features across multiple institutions with varying imaging protocols. Future studies are necessary to further assess the generalizability of the model and to combine additional clinical and advanced imaging features for more robust prediction of survival and progression.

## ACKNOWLEDGMENTS

The authors acknowledge the Ludwig Institute for Cancer Research, Cancer Research Institute, AstraZeneca, and Cure Brain Cancer Foundation for supporting the conduction of the trial, the site investigators and their teams, and the patients and their families for participating in the study.

Disclosure forms provided by the authors are available with the full text and PDF of this article at [www.ajnr.org](http://www.ajnr.org).

## REFERENCES

- Ostrom QT, Cioffi G, Gittleman H, et al. **CBTRUS Statistical Report: Primary Brain and Other Central Nervous System Tumors Diagnosed in the United States in 2012-2016.** *Neuro Oncol* 2019;21:v1-100 [CrossRef Medline](#)
- Stupp R, Hegi ME, Mason WP, et al; European Organisation for Research and Treatment of Cancer Brain Tumour and Radiation Oncology Groups; National Cancer Institute of Canada Clinical Trials Group. **Effects of radiotherapy with concomitant and adjuvant temozolomide versus radiotherapy alone on survival in glioblastoma in a randomised phase III study: 5-year analysis of the EORTC-NCIC trial.** *Lancet Oncol* 2009;10:459-66 [CrossRef Medline](#)
- Lombardi G, Pambuku A, Bellu L, et al. **Effectiveness of antiangiogenic drugs in glioblastoma patients: a systematic review and meta-analysis of randomized clinical trials.** *Crit Rev Oncol Hematol* 2017;111:94-102 [CrossRef Medline](#)
- Wainwright DA, Chang AL, Dey M, et al. **Durable therapeutic efficacy utilizing combinatorial blockade against IDO, CTLA-4, and PD-L1 in mice with brain tumors.** *Clin Cancer Res* 2014;20:5290-301 [CrossRef Medline](#)
- Zeng J, See AP, Phallen J, et al. **Anti-PD-1 blockade and stereotactic radiation produce long-term survival in mice with intracranial gliomas.** *Int J Radiat Oncol Biol Phys* 2013;86:343-49 [CrossRef Medline](#)
- Bristol-Myers Squibb Announces Phase 3 CheckMate-498 Study Did Not Meet Primary Endpoint of Overall Survival with Opdivo (nivolumab) Plus Radiation in Patients with Newly Diagnosed MGMT-Unmethylated Glioblastoma Multiforme. <https://news.bms.com/press-release/corporatefinancial-news/bristol-myers-squibb-announces-phase-3-checkmate-498-study-did>. May 9, 2019. Accessed March 30, 2020
- Bristol-Myers Squibb Provides Update on Phase 3 Opdivo (nivolumab) CheckMate-548 Trial in Patients with Newly Diagnosed MGMT-Methylated Glioblastoma Multiforme. <https://news.bms.com/press-release/corporatefinancial-news/bristol-myers-squibb-provides-update-phase-3-opdivo-nivolumab->. September 5, 2019. Accessed March 30, 2020.
- Reardon DA, Brandes AA, Omuro A, et al. **Effect of nivolumab vs bevacizumab in patients with recurrent glioblastoma: the CheckMate 143 Phase 3 randomized clinical trial.** *JAMA Oncol* 2020;6:1003-10 [CrossRef Medline](#)
- Reardon DA, Kaley TJ, Dietrich J, et al. **Phase 2 study to evaluate safety and efficacy of MEDI4736 (durvalumab [DUR]) in glioblastoma (GBM) patients: an update.** *J Clin Oncol* 2017;35:2042 [CrossRef](#)
- Huang RY, Wen PY. **Response assessment in neuro-oncology criteria and clinical endpoints.** *Magn Reson Imaging Clin N Am* 2016;24:705-18 [CrossRef Medline](#)
- Okada H, Weller M, Huang R, et al. **Immunotherapy response assessment in neuro-oncology: a report of the RANO working group.** *Lancet Oncol* 2015;16:e534-42 [CrossRef Medline](#)
- Reardon DA, Omuro A, Brandes AA, et al. **OS10.3 randomized Phase 3 study evaluating the efficacy and safety of nivolumab vs bevacizumab in patients with recurrent glioblastoma: CheckMate 143.** *Neuro Oncol* 2017;19:iii21 [CrossRef](#)
- Phase 2 Study of Durvalumab (MEDI4736) in Patients With Glioblastoma.** <https://clinicaltrials.gov/ct2/show/NCT02336165>. Accessed February 1, 2022
- Reardon DA, Kaley TJ, Dietrich J, et al. **Phase II study to evaluate safety and efficacy of MEDI4736 (durvalumab) + radiotherapy in patients with newly diagnosed unmethylated MGMT glioblastoma (new unmeth GBM).** *J Clin Oncol* 2019;37(15 Suppl):2032 [CrossRef](#)
- Zwanenburg A, Leger S, Vallieres M, et al. **Image biomarker standardisation initiative.** <https://arxiv.org/abs/1612.07003>. December 2, 2016. Accessed February 1, 2022
- Documentation/Nightly/Modules/SwissSkullStripper.** <https://www.slicer.org/wiki/Documentation/Nightly/Modules/SwissSkullStripper>. Accessed February 1, 2022
- Chang K, Zhang B, Guo X, et al. **Multimodal imaging patterns predict survival in recurrent glioblastoma patients treated with bevacizumab.** *Neuro Oncol* 2016;18:1680-87 [CrossRef Medline](#)
- Vallières M, Freeman CR, Skamene SR, et al. **A radiomics model from joint FDG-PET and MRI texture features for the prediction of lung metastases in soft-tissue sarcomas of the extremities.** *Phys Med Biol* 2015;60:5471-96 [CrossRef Medline](#)
- Vallieres M, Kay-Rivest E, Perrin LJ, et al. **Radiomics strategies for risk assessment of tumour failure in head-and-neck cancer.** *Sci Rep* 2017;7:10117 [CrossRef Medline](#)
- A repository to develop code for IBSI compliant radiomics applications.** <https://github.com/mvallieres/radiomics-develop>. Accessed April 26, 2020
- Ishwaran H, Kogalur UB, Blackstone EH, et al. **Random survival forests.** *Annals of Applied Statistics* 2008;2:841-60
- scikit-survival.** <https://scikit-survival.readthedocs.io/en/stable/>. Accessed February 1, 2022
- Hung H, Chiang C. **Estimation methods for time-dependent AUC models with survival data.** *The Canadian Journal of Statistics* 2009;38:8-26
- Rundo F, Spampinato C, Banna GL, et al. **Advanced deep learning embedded motion radiomics pipeline for predicting anti-PD-1/**

- PD-L1 immunotherapy response in the treatment of bladder cancer: preliminary results.** *Electronics* 2019;8:1134 [CrossRef](#)
25. Jazieh K, Khorrami M, Saad AM, et al. **Novel imaging biomarkers predict progression-free survival in stage 3 NSCLC treated with chemoradiation and durvalumab.** *J Clin Oncol* 2021;39(15 Suppl):3054–54 [CrossRef](#)
  26. Sforazzini F, Salome P, Kudak A, et al. **PD-L1-R: A MR based surrogate for PD-L1 expression in glioblastoma multiforme.** *J Clin Oncol* 2021;39:2041 [CrossRef](#)
  27. Lotan E, Jain R, Razavian N, et al. **State of the art: machine learning applications in glioma imaging.** *AJR Am J Roentgenol* 2019;212:26–37 [CrossRef Medline](#)
  28. Sengupta A, Ramaniharani AK, Gupta RK, et al. **Glioma grading using a machine-learning framework based on optimized features obtained from T1 perfusion MRI and volumes of tumor components.** *J Magn Reson Imaging* 2019;50:1295–1306 [CrossRef Medline](#)
  29. Zhang B, Chang K, Ramkissoon S, et al. **Multimodal MRI features predict isocitrate dehydrogenase genotype in high-grade gliomas.** *Neuro Oncol* 2017;19:109–17 [CrossRef Medline](#)
  30. Chang K, Beers AL, Bai HX, et al. **Automatic assessment of glioma burden: a deep learning algorithm for fully automated volumetric and bidimensional measurement.** *Neuro Oncol* 2019;21:1412–22 [CrossRef Medline](#)
  31. Macyszyn L, Akbari H, Pisapia JM, et al. **Imaging patterns predict patient survival and molecular subtype in glioblastoma via machine learning techniques.** *Neuro Oncol* 2016;18:417–25 [CrossRef Medline](#)
  32. Sanghani P, Ang BT, King NK, et al. **Overall survival prediction in glioblastoma multiforme patients from volumetric, shape and texture features using machine learning.** *Surg Oncol* 2018;27:709–14 [CrossRef Medline](#)
  33. Kickingereder P, Burth S, Wick A, et al. **Radiomic profiling of glioblastoma: identifying an imaging predictor of patient survival with improved performance over established clinical and radiologic risk models.** *Radiology* 2016;280:880–89 [CrossRef Medline](#)
  34. Grossmann P, Narayan V, Chang K, et al. **Quantitative imaging biomarkers for risk stratification of patients with recurrent glioblastoma treated with bevacizumab.** *Neuro Oncol* 2017;19:1688–97 [CrossRef Medline](#)
  35. Kickingereder P, Gotz M, Muschelli J, et al. **Large-scale radiomic profiling of recurrent glioblastoma identifies an imaging predictor for stratifying anti-angiogenic treatment response.** *Clin Cancer Res* 2016;22:5765–71 [CrossRef Medline](#)
  36. Wang C, Sun W, Kirkpatrick J, et al. **Assessment of concurrent stereotactic radiosurgery and bevacizumab treatment of recurrent malignant gliomas using multi-modality MRI imaging and radiomics analysis.** *J Radiosurg SBRT* 2018;5:171–81 [Medline](#)
  37. Nie D, Lu J, Zhang H, et al. **Multi-channel 3D deep feature learning for survival time prediction of brain tumor patients using multi-modal neuroimages.** *Sci Rep* 2019;9:1103 [CrossRef Medline](#)
  38. Zhao J, Chen AX, Gartrell RD, et al. **Immune and genomic correlates of response to anti-PD-1 immunotherapy in glioblastoma.** *Nat Med* 2019;25:462–69 [CrossRef Medline](#)
  39. Lipson EJ, Forde PM, Hammers HJ, et al. **Antagonists of PD-1 and PD-L1 in cancer treatment.** *Semin Oncol* 2015;42:587–600 [CrossRef Medline](#)
  40. De Felice F, Pranno N, Marampon F, et al. **Immune check-point in glioblastoma multiforme.** *Crit Rev Oncol Hematol* 2019;138:60–69 [CrossRef Medline](#)
  41. Burugu S, Dancsok AR, Nielsen TO. **Emerging targets in cancer immunotherapy.** *Semin Cancer Biol* 2018;52:39–52 [CrossRef Medline](#)